Mass and heat transfer by natural convection in a vertical cavity

A. Bejan*

This paper reports a fundamental study of laminar natural convection in a rectangular enclosure with heat and mass transfer from the side, when the buoyancy effect is due to density variations caused by either temperature or concentration variations. In the first part of the study scale analysis is used to determine the scales of the flow, temperature and concentration fields in boundary layer flow for all values of Prandtl and Lewis numbers. In particular, scale analysis shows that in the extreme case where the flow is driven by buoyancy due to temperature variations, the ratio of mass transfer rate divided by heat transfer rate scales as $Le^{1/2}$ only if ($Pr>1, Le<1$) or ($Pr<1, Sc<1$), and as $Le^{1/3}$ if ($Pr>1, Le>1$) or ($Pr<1$, $Sc>1$). In the second part of the study, the boundary layer scales derived in the first part are used to determine the heat and mass transport characteristics of a vertical slot filled with fluid. Criteria for the existence of distinct thermal and concentration boundary layers in the slot are determined. Numerical solutions for the flow and concentration fields in a slot without distinct thermal boundary layers are reported. These solutions support further the method of scale analysis employed in the first part of the study

Keywords: *convection, heat transfer, mass transfer, scale analysis*

This paper reports a fundamental study of natural convection in a vertical cavity filled with fluid, when the buoyancy effect is due to density variations caused by heat and mass transfer along the vertical sides of the cavity. Related to environmental applications involving the transport of water vapour and other chemical contaminants across enclosed spaces, the focus of the work is on the boundary layer regime in which the rates of heat and mass transfer across the enclosure can greatly exceed the estimates based on the assumption of pure diffusion.

Although the objective of this study is the boundary layer regime in the enclosures configuration, the first part is devoted to a detailed analysis of the scales describing the flow, temperature and concentration fields in the immediate vicinity of a single vertical wall immersed in a fluid reservoir with different temperature and concentration. Two decades of intensive research on enclosures in the presence of only heat transfer have shown that a theoretical understanding of the proper scales of enclosure flows is tied closely to the understanding of the scales of natural convection in isolated boundary layer flow[1]. The same conclusion emerges in the parallel field of heat-transfer-driven natural convection in porous media[2]. An additional reason for sorting out the scales of a boundary layer first is that, currently, these scales are known only for flows in relatively narrow ranges of Prandtl and Schmidt numbers[3-7]. Scaling work in the entire (Pr, Sc) domain is needed to convey an effective overview of the heat and mass transfer natural convection phenomenon.

* Department of Mechanical Engineering and Materials Science, Duke University, Durham, NC 27706, USA
Received 10 October 1984 and accepted for publication on 31 January 1985

The boundary layer scales thus revealed are used to determine criteria for the existence of the boundary layer regime in an enclosure, that is, criteria for the correctness of using the heat and mass transfer scales of the boundary layer in order to evaluate the transport capability of the enclosure. The study concludes with numerical experiments focusing on the intermediate regime where only one boundary layer (temperature or concentration) is distinct, the other transfer process being governed by pure diffusion.

Boundary layer formulation

Consider the two-dimensional flow in the immediate vicinity of a vertical wall (Fig 1). The wall and the unaffected fluid reservoir are maintained at different temperatures, T_0 and T_∞, while the concentration of a certain constituent varies from C_0 on the fluid side of the wall to C_∞ sufficiently far into the fluid reservoir. The vertical boundary layer flow is driven by the buoyancy effect associated with the density difference between wall fluid and reservoir fluid. The boundary layer momentum equation for this flow is:

$$u\frac{\partial v}{\partial x}+v\frac{\partial v}{\partial y}=\nu\frac{\partial^2 v}{\partial x^2}+\frac{g}{\rho}(\rho_\infty-\rho) \quad (1)$$

where u and v are the local velocity components, and g, ν, ρ and ρ_∞ are the gravitational acceleration, kinematic viscosity, density and reservoir fluid density, respectively. Since the thermodynamic state of the fluid mixture depends on pressure, temperature and composition, in the limit of small density variations at constant pressure we can write:

$$\rho\cong\rho_\infty-\rho\beta(T-T_\infty)-\rho\beta_C(C-C_\infty) \quad (2)$$

 0142-727X/85/030149-11$3.00

where β and β_C are the thermal and concentration expansion coefficients:

$$\beta = -\frac{1}{\rho}\left(\frac{\partial \rho}{\partial T}\right)_P \qquad \beta_C = -\frac{1}{\rho}\left(\frac{\partial \rho}{\partial C}\right)_P \tag{3}$$

Based on the approximation in Eq (2) the boundary layer momentum equation (1) becomes:

$$u\frac{\partial v}{\partial x} + v\frac{\partial v}{\partial y} = \nu\frac{\partial^2 v}{\partial x^2} + g\beta(T - T_\infty) + g\beta_C(C - C_\infty) \tag{4}$$

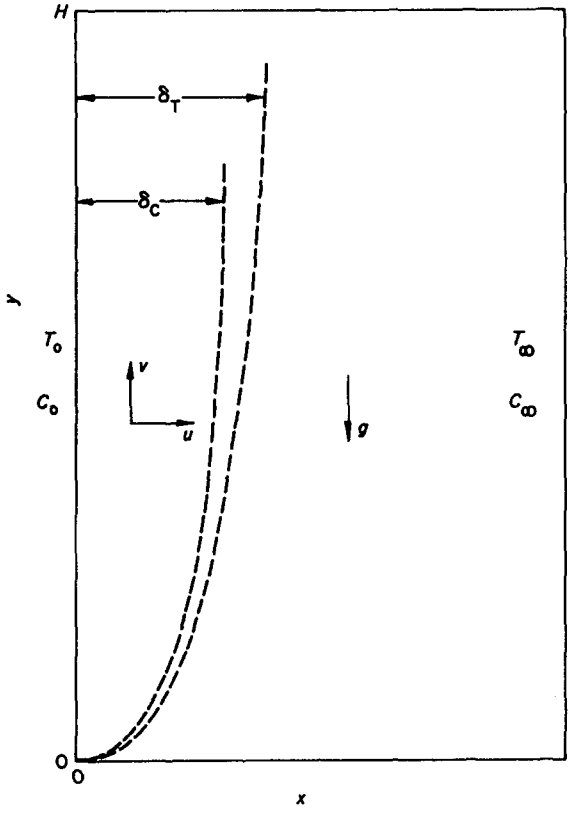

Fig 1 Thermal and concentration boundary layers near a vertical wall

The flow is thus linearly coupled to the temperature and concentration fields obtained by solving the boundary layer energy and concentration equations:

$$u\frac{\partial T}{\partial x} + v\frac{\partial T}{\partial y} = \alpha\frac{\partial^2 T}{\partial x^2} \tag{5}$$

$$u\frac{\partial C}{\partial x} + v\frac{\partial C}{\partial y} = D\frac{\partial^2 C}{\partial x^2} \tag{6}$$

where T, α, C and D are the boundary layer fluid temperature, thermal diffusivity, concentration (expressed as kilograms of constituent per unit volume) and mass diffusivity of constituent through the fluid mixture, respectively. The appropriate boundary conditions for the boundary layer-approximated equations (4)–(6) are:

$$u = 0 \qquad v = 0 \qquad T = T_0 \qquad C = C_0 \qquad \text{at } x = 0 \tag{7}$$

$$v = 0 \qquad T = T_\infty \qquad C = C_\infty \qquad \text{as } x \to \infty \tag{8}$$

The fourth equation needed for determining uniquely the four unknowns of the boundary layer problem (u, v, T, C) is the mass conservation equation:

$$\frac{\partial u}{\partial x} + \frac{\partial v}{\partial y} = 0 \tag{9}$$

The boundary layer flow is subjected to scale analysis below; however, in order to give structure to this analysis it is helpful to recognize two important extremes in which the phenomenon can exist. Comparison of the scales of the two buoyancy terms in the momentum equation suggests two classes of flows:

(i) Heat-transfer-driven flows when the buoyancy effect due to heating from the side dominates:

$$|\beta(T_0 - T_\infty)| \gg |\beta_C(C_0 - C_\infty)| \tag{10}$$

(ii) Mass-transfer-driven flows, when the buoyancy due to heating from the side is negligible:

$$|\beta(T_0 - T_\infty)| \ll |\beta_C(C_0 - C_\infty)| \tag{11}$$

The use of absolute-value notation in Eqs (10) and (11) is a reminder that parameters β, ΔT, β_C and ΔC can be positive

Notation

C	Concentration
D	Mass diffusivity
g	Gravitational acceleration
H	Height of vertical wall or cavity
j''	Mass flux, Eq (48)
J	Overall mass transfer rate, Eq (14)
L	Horizontal dimension of cavity
Le	Lewis number, Eq (19)
N	Buoyancy ratio, Eq (12)
Nu	Overall Nusselt number, Eq (13)
P	Pressure
Pr	Prandtl number, Eq (13)
Q	Overall heat transfer rate, Eq (13)
Ra	Rayleigh number, Eq (13)
Ra_m	Rayleigh number, mass-transfer-driven flows, Eq (46)
Ra_y	Local Rayleigh number, Eq (48)
Sc	Schmidt number, Eq (28)
Sh	Sherwood number, Eq (14)
Sh_y	Local Sherwood number, Eq (48)
T	Temperature
u	Horizontal velocity
v	Vertical velocity
x	Horizontal coordinate
y	Vertical coordinate
α	Thermal diffusivity
β	Thermal expansion coefficient
β_C	Concentration expansion coefficient
δ_C	Concentration boundary layer thickness
δ_T	Thermal boundary layer thickness
δ_v	Viscous shear layer thickness
ν	Kinematic viscosity
ρ	Density
ω	Vorticity
ψ	Streamfunction
$(\,)_0$	Wall property
$(\,)_\infty$	Fluid reservoir property
$\Delta(\,)$	Difference
$(\hat{\ })$	Dimensionless variables, Eq (68)

Table 1 Summary of flow and heat transfer scales in natural convection boundary layer flow driven by buoyancy due to heating from the side

Prandtl number range	Thermal boundary layer thickness	Velocity profile scales: Vertical velocity	Velocity profile scales: Overall thickness of wall jet	Velocity profile scales: Distance from wall to velocity peak	Nusselt number $Nu \sim H/\delta_T$	Fig
$Pr > 1$	$HRa^{-1/4}$	$\frac{\alpha}{H} Ra^{1/2}$	$HRa^{-1/4} Pr^{1/2}$	$HRa^{-1/4}$	$Ra^{1/4}$	Figs 2(a)–(c)
$Pr < 1$	$HRa^{-1/4} Pr^{-1/4}$	$\frac{\alpha}{H} Ra^{1/2} Pr^{1/2}$	$HRa^{-1/4} Pr^{-1/4}$	$HRa^{-1/4} Pr^{1/4}$	$Ra^{1/4} Pr^{1/4}$	Figs 2(d)–(f)

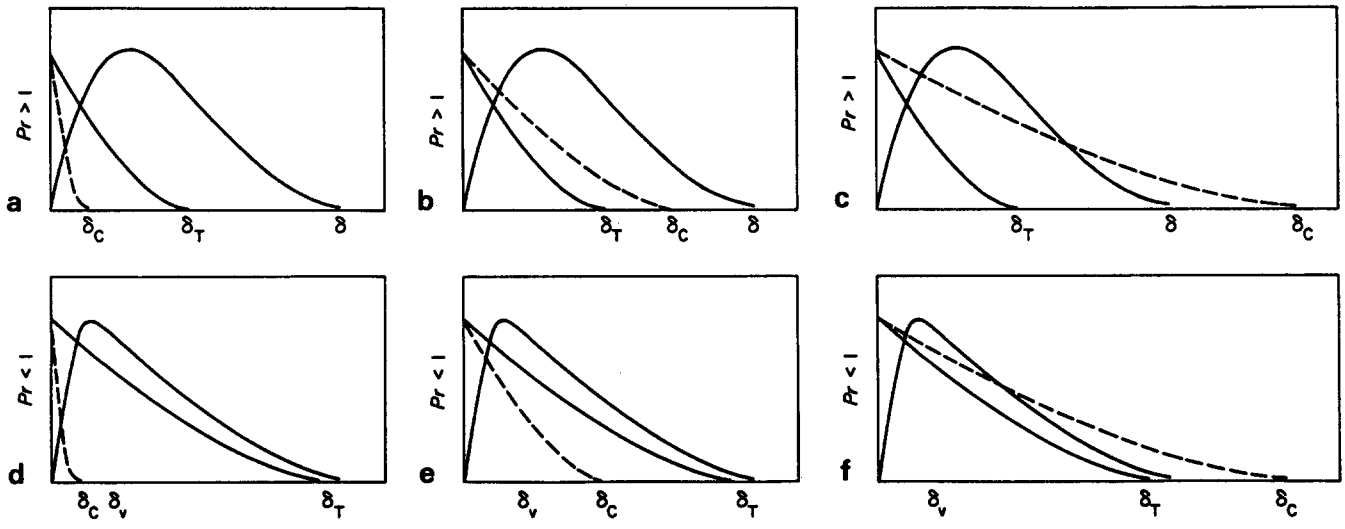

Fig 2 Relative size of velocity, temperature and concentration boundary layer thicknesses in heat-transfer-driven natural convection (Tables 1 and 2)

or negative. The distinction between these flows can also be made using the 'buoyancy ratio';

$$N = \frac{\beta_C (C_0 - C_\infty)}{\beta (T_0 - T_\infty)} \tag{12}$$

hence $|N| < 0(1)$ for class (i), and $|N| > 0(1)$ for class (ii).

Heat-transfer-driven flows

The object of scale analysis is to determine the order of magnitude of flow velocities normal to and along the wall, and the order of magnitude of the four boundary layer thicknesses that characterize the phenomenon (two thicknesses for the velocity layer, one for the thermal layer, and one for the concentration layer). This analysis begins with heat-transfer-driven flows because the velocity and heat transfer scales of such flows are known already: a summary of these scales is presented in Table 1, based on articles published by Patterson and Imberger[1], and Bejan and Cunnington[8], using the notation:

$$Ra = \frac{g\beta\, \Delta T H^3}{\alpha \nu} \quad \text{Rayleigh number}$$

$$Pr = \nu/\alpha \quad \text{Prandtl number} \tag{13}$$

$$Nu = \frac{Q}{k\, \Delta T} \quad \text{Nusselt number}$$

where Q is the overall heat transfer rate from the wall of height H, per unit length normal to the plane of Fig 1; note that $Q \sim kH\, \Delta T/\delta_T$, where δ_T is the thermal boundary layer thickness scale.

It remains to establish the concentration boundary layer thickness compatible with heat-transfer-driven flows, hence, the overall Sherwood number:

$$Sh = \frac{J}{D\, \Delta C} \sim \frac{H}{\delta_C} \tag{14}$$

where δ_C is the concentration boundary layer thickness, and J is the overall mass transfer rate from the wall of height H, per unit length normal to the plane of Fig 1 ($J \sim DH\, \Delta C/\delta_C$). As shown in Fig 2, there are six distinct possibilities depending on the Prandtl number and on the relative size of δ_C and the two length scales of the heat-transfer-driven wall jet.

Case (a): Pr > 1 and $\delta_C < \delta_T$

In the boundary layer region of height H and thickness δ_C shown in Fig 2(a), the constituent conservation equation (6) requires:

$$\frac{v}{H} \sim \frac{D}{\delta_C^2} \tag{15}$$

Since δ_C is much smaller than the thermal boundary layer

thickness $\delta_T \sim HRa^{-1/4}$ (Table 1), the vertical velocity scale in the δ_C-thick layer is only a fraction of the velocity scale of the thermal boundary layer:

$$v \sim \frac{\delta_C}{\delta_T}\frac{\alpha}{H} Ra^{1/2} \tag{16}$$

Combining Eqs (15) and (16):

$$\delta_C \sim H\, Le^{-1/3}\, Ra^{-1/4} \tag{17}$$

$$Sh \sim Le^{1/3}\, Ra^{1/4} \tag{18}$$

where Le is the Lewis number defined as:

$$Le = \frac{\alpha}{D} \tag{19}$$

To end case (a), note that scales (17) and (18) are valid if $\delta_C < \delta_T$, ie, if:

$$Le > 1 \tag{20}$$

Therefore, case (a) corresponds to fluids with both Prandtl and Lewis numbers of order one or greater.

Case (b): Pr> *1 and* $\delta_T < \delta_C < \delta$

When the concentration layer is thicker than the thermal boundary layer, the vertical velocity scale inside the δ_C-thick layer is the same as that inside the velocity layer of thickness $\delta \sim H\, Ra^{-1/4}\, Pr^{1/2}$ (Table 1):

$$v \sim \frac{\alpha}{H} Ra^{1/2} \tag{21}$$

Eqs (15) and (21) could be combined to determine the δ_C scale; a more instructive alternative, however, is first to integrate the constituent conservation equation (6) across the boundary layer:

$$\frac{\mathrm{d}}{\mathrm{d}y}\int_0^\infty v(C - C_\infty)\,\mathrm{d}x = -D\left(\frac{\partial C}{\partial x}\right)_{x=0} \tag{22}$$

and to recognize that this integral condition implies a balance between diffusive mass transfer from the side and vertical upflow of the constituent of interest:

$$\frac{v\,\Delta C}{H}\min(\delta_C, \delta) \sim D\frac{\Delta C}{\delta_C} \tag{23}$$

A critical observation that forms the basis for distinguishing between cases (b) and (c), discussed next, is that the scale of x in Eq (22) is the smaller of δ_C and δ [note that the vertical upflow of constituent must occupy a boundary layer region that has upward flow, $0 \leqslant x \leqslant \delta$, and high concentration of constituent, $0 \leqslant x \leqslant \delta_C$: that region is $0 \leqslant x \leqslant \min(\delta_C, \delta)$]. Therefore, using $v\,\Delta C\delta_C/H$ as the left-hand side of Eq (23), and since the v-scale is known from Table 1, we have the means to determine the mass transfer scales of case (b):

$$\delta_C \sim H\, Le^{-1/2}\, Ra^{-1/4} \tag{24}$$

$$Sh \sim Le^{1/2}\, Ra^{1/4} \tag{25}$$

The above scales hold provided:

$$\delta_T \leqslant \delta_C \leqslant \delta \tag{26}$$

in other words when:

$$Le < 1 < Sc \tag{27}$$

where Sc is the Schmidt number:

$$Sc = Pr\, Le \tag{28}$$

The domain of validity of scales (24) and (25) is shown on the Le–Pr plane of Fig 3.

Case (c): Pr> *1 and* $\delta_C > \delta$

When the concentration boundary layer is thicker than the velocity profile, we use $v\,\Delta C\delta/H$ on the left-hand side of Eq (23) and the resulting mass transfer scales are:

$$\delta_C \sim H\, Le^{-1}\, Ra^{-1/4}\, Pr^{-1/2} \tag{29}$$

$$Sh \sim Le\, Ra^{1/4}\, Pr^{1/2} \tag{30}$$

The validity condition for these scales is the assumed inequality $\delta_C > \delta$, which translates into:

$$Sc < 1 \tag{31}$$

Thus the domain covered by case (c) is delineated by $Pr > 1$ and $Sc < 1$ in Fig 3 (note that in this domain Le is smaller than one).

Case (d): Pr< *1 and* $\delta_C < \delta_v$

In liquid metals the outer thickness of the velocity profile scales as the thermal boundary layer thickness. Consider a concentration boundary layer much thinner than the viscous shear layer whose thickness (Table 1) is:

$$\delta_v \sim H\, Ra^{-1/4}\, Pr^{1/4} \tag{32}$$

In the concentration layer of thickness δ_C and height H, the vertical velocity scale is only a fraction of the velocity scale inside the thermal boundary layer:

$$v \sim \left(\frac{\delta_C}{\delta_v}\right)\left(\frac{\alpha}{H} Ra^{1/2}\, Pr^{1/2}\right) \tag{33}$$

therefore, the constituent conservation balance (15) requires

$$\delta_C \sim H\, Le^{-1/3}\, Ra^{-1/4}\, Pr^{-1/12} \tag{34}$$

$$Sh \sim Le^{1/3}\, Ra^{1/4}\, Pr^{1/12} \tag{35}$$

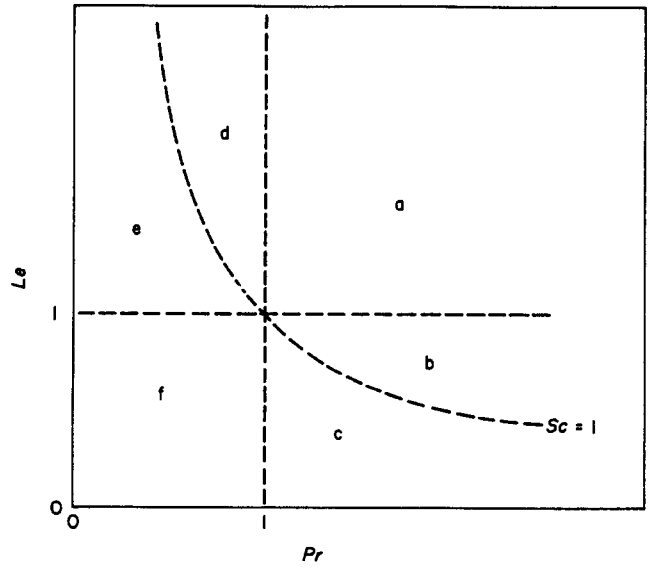

Fig 3 The domains in which the mass transfer scales of heat-transfer-driven flows are valid (Table 2)

Writing $\delta_C \ll \delta_v$, we find that scales (34) and (35) are valid if:

$$Sc > 1 \tag{36}$$

Case (e): Pr < 1 and $\delta_v < \delta_C < \delta_T$

Considering again the balance between mass transfer from the side and constituent upflow, Eq (22), we conclude that:

$$\frac{v\,\Delta C}{H}\min(\delta_C, \delta_T) \sim D\frac{\Delta C}{\delta_C} \tag{37}$$

In case (e) the smaller of δ_C and δ_T is δ_C; therefore, using δ_C on the left hand side of Eq (37) and $v \sim (\alpha/H)Ra^{1/2}\,Pr^{1/2}$ (Table 1) yields:

$$\delta_C \sim H\,Le^{-1/2}\,Ra^{-1/4}\,Pr^{-1/4} \tag{38}$$

$$Sh \sim Le^{1/2}Ra^{1/4}Pr^{1/4} \tag{39}$$

As validity conditions for the above scales we write $\delta_v < \delta_C < \delta_T$, and the result is:

$$Sc < 1 < Le \tag{40}$$

The domain defined by these conditions is shown labeled (e) in Fig 3.

Case (f): Pr < 1 and $\delta_C > \delta_T$

Finally, in the case of small Lewis numbers the concentration layer may extend beyond the thermal boundary layer (Fig 2(f)). Therefore, starting with $v\,\Delta C\delta_T/H$ on the left-hand side of Eq (37) leads to the following mass transfer scales:

$$\delta_C \sim H\,Le^{-1}\,Ra^{-1/4}\,Pr^{-1/4} \tag{41}$$

Table 2 Summary of mass transfer scales in natural convection boundary layer flow driven by buoyancy due to heating from the side

Configuration (Fig 2)	Sherwood number $Sh \sim H/\delta_c$	Domain of validity (Fig 3)		
		Pr	*Le*	*Sc*
(a)	$Le^{1/3}Ra^{1/4}$	>1	>1	>1
(b)	$Le^{1/2}Ra^{1/4}$	>1	<1	>1
(c)	$LeRa^{1/4}Pr^{1/2}$	>1	<1	<1
(d)	$Le^{1/3}Ra^{1/4}Pr^{1/12}$	<1	>1	>1
(e)	$Le^{1/2}Ra^{1/4}Pr^{1/4}$	<1	>1	<1
(f)	$LeRa^{1/4}Pr^{1/4}$	<1	<1	<1

$$Sh \sim Le\,Ra^{1/4}\,Pr^{1/4} \tag{42}$$

As validity condition we have the assumption $\delta_C > \delta_T$, which means:

$$Le < 1 \tag{43}$$

The square subdomain labeled (f) on Fig 3 completes the scale analysis of mass transfer to heat-transfer-driven natural convection boundary layer flow. The mass transfer scales revealed by this analysis are summarized in Table 2 with their respected domains of validity. Noting that from case (a) to case (f), all the Sherwood number scales are different: the existence of six *Sh* scales for heat-transfer-driven flows alone stresses the need for having undertaken the scale analysis of the phenomenon, without restrictions on the size of the *Pr* and *Sc* domains.

Mass-transfer-driven flows

This section considers the second class of boundary layer flows (identified as (ii) earlier), wall-jet flows driven by buoyancy associated mainly with the variation of concentration. The scales of the flow, temperature and concentration fields may be derived by repeating step-by-step the scale analysis used above. However it is sufficient to note that the scale analysis of mass-transfer-driven flows can be written by simply subjecting the analysis above to the transformation

$$\begin{aligned} \beta\,\Delta T &\rightarrow \beta_C\,\Delta C \\ \alpha &\rightleftarrows D \\ \delta_T &\rightleftarrows \delta_C \end{aligned} \tag{44}$$

Related to the dimensionless groups that influence the flow and transfer scales of the phenomenon, this transformation means:

$$\begin{aligned} Pr &\rightleftarrows Sc \\ Ra &\rightarrow Ra_m \\ Le &\rightarrow Le^{-1} \\ Nu &\rightleftarrows Sh \end{aligned} \tag{45}$$

where Ra_m is the 'mass-transfer' Rayleigh number obtained by subjecting *Ra* to transformation (44):

$$Ra_m = \frac{g\beta_C\,\Delta C H^3}{\nu D} = Ra\,Le\,N \tag{46}$$

The value of this observation is that the scales of mass-transfer-driven flows can now be deduced by combining Tables 1 and 2 with the dimensionless transformation (45). The resulting scales are summarized in Tables 3 and 4. It is

Table 3 Summary of flow and mass transfer scales in natural convection boundary layer flow driven by mass transfer from the side

Schmidt number range	Concentration boundary layer thickness	Velocity profile scales			Sherwood number $Sh \sim H/\delta_c$
		Verticial velocity	Overall thickness of wall jet	Distance from wall to velocity peak	
$Sc > 1$	$HRa_m^{-1/4}$	$\frac{D}{H}Ra_m^{1/2}$	$HRa_m^{-1/4}Sc^{1/2}$	$HRa_m^{-1/4}$	$Ra_m^{1/4}$
$Sc < 1$	$HRa_m^{-1/4}Sc^{-1/4}$	$\frac{D}{H}Ra_m^{1/2}Sc^{1/2}$	$HRa_m^{-1/4}Sc^{-1/4}$	$HRa_m^{-1/4}Sc^{1/4}$	$Ra_m^{1/4}Sc^{1/4}$

Table 4 Summary of heat transfer scales in natural convection boundary layer flow driven by buoyancy due to mass transfer from the side

Configuration	Nusselt number, $Nu \sim H/\delta_T$	Domain of validity (Fig 4)		
		Pr	*Le*	*Sc*
(g)	$Le^{-1/3}Ra_m^{1/4}$	>1	<1	>1
(h)	$Le^{-1/2}Ra_m^{1/4}$	>1	>1	>1
(i)	$Le^{-1}Ra_m^{1/4}Sc^{1/2}$	<1	>1	>1
(j)	$Le^{-1/3}Ra_m^{1/4}Sc^{1/12}$	>1	<1	<1
(k)	$Le^{-1/2}Ra_m^{1/4}Sc^{1/4}$	<1	<1	<1
(l)	$Le^{-1}Ra_m^{1/4}Sc^{1/4}$	<1	>1	<1

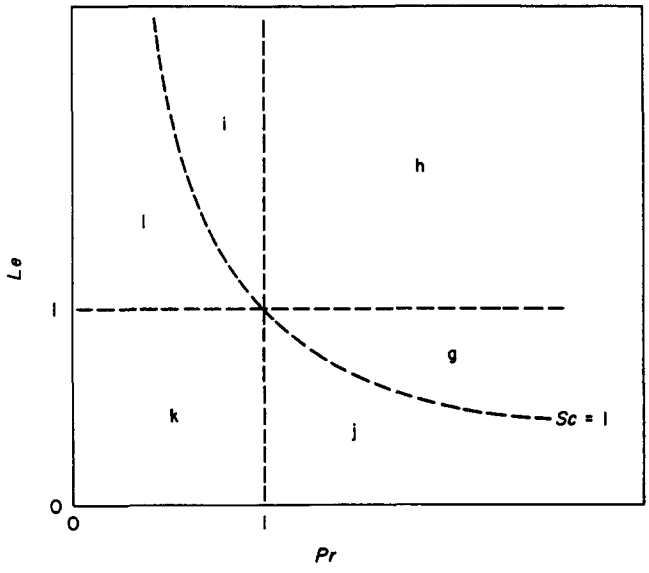

Fig 4 The domains in which the heat transfer scales of mass-transfer-driven flows are valid (Table 4)

worth considering the symmetry of Tables 1 and 3 and Tables 2 and 4, and noting that in mass-transfer-driven flows the Schmidt number plays the role played by the Prandtl mumber for heat-transfer-driven flows. Note also that in either class of flows, (i) or (ii), there are only two scaling patterns (possibilities) for the flow and the transfer process that drives the flow. In either class, there are six different scaling patterns for the transfer process that does not contribute to the buoyancy effect driving the flow. In flows of class (ii), the six possible ways of estimating the heat transfer scale are presented as cases (g)–(l) in Table 4 and Fig 4.

Discussion of scaling results

The complexity of combined heat and mass transfer in vertical boundary layer natural convection is amply illustrated by the numerous scales organized in Tables 1–4. The Nusselt number, for example, is always proportional to $Ra^{1/4}$ (Tables 1 and 4); however, the coefficient in this proportionality can have eight different expressions depending on *N*, *Pr* and *Le* (or *Sc*). The same is true for the Sherwood number scales summarized in Tables 2 and 3. Obviously, comparisons of the results of scale analysis with published analytical and experimental results must be approached with caution.

The literature contains a number of studies of the combined boundary layer problem of Fig 1. However, these studies are not conclusive with respect to how the mass transfer rate varies vis-à-vis the heat transfer rate, ie on how the ratio *Sh/Ra* depends on *Le*. The main reason for this state of affairs is that, with one exception[7], the existing studies address a limited range of Prandtl numbers and Schmidt numbers. For example, the first integral analysis of the phenomenon[3] is valid only for *Pr* and *Sc* values of order 0(1). Nevertheless, Somers' analysis[3] indicates that *Sh/Ra* must scale as $Le^{1/2}$ when the flow is dominated by the buoyancy effect due to heating from the side. This conclusion is in qualitative (average) agreement with the *Le* dependence recommended by the results listed as (a)–(f) in Table 2 (since *Pr*, *Sc* and *Le* are all of order one, Somers' analysis cannot be compared with a specific case in Table 2). The Lewis number scaling envisioned by Somers is supported by subsequent studies reported by Mathers *et al*[4], Wilcox[5] and deLeeuw Den Bouter *et al*[6].

The scaling conclusions above can be tested partially using Gebhart and Pera's study[7] in which similarity solutions are reported for a wide range of Schmidt numbers, 0.1–500, for both air ($Pr=0.7$) and water ($Pr=7$). At first glance, the difficulty with using Gebhart and Pera's data is that all the flows documented by them fall between class (i) $|N| \ll 1$, and class (ii), $|N| \gg 1$; in other words, all these flows are the result of 'combined' buoyancy effects, either aiding or opposing each other. Indeed, Gebhart and Pera chose to set *N* equal to $-0.5, 0.5, 1$ or 2, in order to document the intermediate range of transition from opposing to aiding buoyancy effects.

Gebhart and Pera's data are in fact quite useful in the present study, because they are numerous enough so that the data for $N=0$ (heat-transfer-driven flow limit) can be deduced with a reasonable degree of accuracy by graphic interpolation. The results of this graphic work are listed in Table 5, where $C'(0)$ is Gebhart and Pera's notation for dimensionless concentration gradient at the wall. In the present notation, $C'(0)$ is proportional to the numerical coefficient in the expected proportionality

Table 5 Mass transfer results for heat-transfer-driven flows ($N=0$), deduced via graphic interpolation from the similarity solutions of Gebhart and Pera[7]

Pr	*Sc*	*Le*	$-C'(0)$	$Sh_y Ra_y^{-1/4}$
7	1	0.143	≈0.4	0.172
	7	1	1.05411	0.458
	100	14.3	~2.95	1.282
	500	71.4	~5.125	2.228
0.7	0.1	0.143	≈0.182	0.141
	0.5	0.714	~0.412	0.318
	0.7	1	0.4995	0.386
	0.94	1.343	~0.579	0.448
	5	7.14	~1.19	0.920
	10	14.3	~1.55	1.20

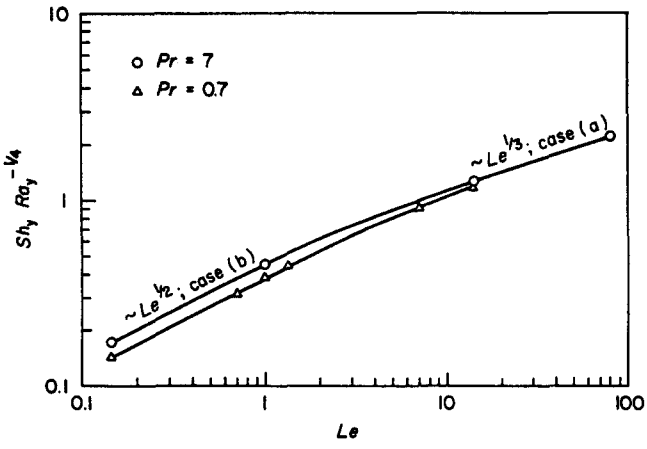

Fig 5 The effect of Lewis number on mass transfer in heat-transfer-driven natural convection boundary layer flow

$$Sh_y \sim Ra_y^{1/4}$$

$$Sh_y = -2^{-1/2} C'(0)\, Pr^{-1/4}\, Ra_y^{1/4} \tag{47}$$

Sh_y and Ra_y are the local Sherwood and Rayleigh numbers:

$$Sh_y = \frac{j''}{\Delta C}\frac{y}{D} \qquad Ra_y = \frac{g\beta \Delta T y^3}{\alpha \nu} \tag{48}$$

where j'' is the local mass flux through the vertical wall. In Table 5, the values determined graphically for $C'(0)$ are preceded by '$\approx$' if the interpolation was based on three points, by '$\sim$' if based on four points, and by no sign if the value was reported numerically by Gebhart and Pera[7].

Fig. 5 shows the $N=0$ data of Table 5 plotted as $Sh_y\, Ra_y^{-1/4}$ versus Le; the data spans the Lewis number range 0.1–100, while the Prandtl number is either 0.7 or 7. Fig 5 is thus an ideal test for the results listed as (a) and (b) in Table 2, regarding the Prandtl numbers 0.7 and 7 as of order unity or greater. The data show convincingly that at small Lewis numbers the scaling law is $Sh_y \sim Le^{1/2} Ra_y^{1/4}$, in agreement with result (b) of Table 2 (note that the two left most points on each curve in Fig 5 are united by a straight line drawn intentionally with a slope of 1/2). At large Lewis numbers, the scaling law changes visibly to $Sh_y \sim Le^{1/3} Ra_y^{1/4}$, as the two right most points fall on a line of slope 1/3. This last feature validates result (a) of Table 2. And, the transition from one scaling law to the other takes place in the vicinity of $Le = O(1)$, which is in agreement with the transition between subdomains (a) and (b) in Fig 3.

The test illustrated in Fig 5 shows also the negligible effect of Prandtl number on the $Sh_y \sim Ra_y^{1/4}$ proportionality: this finding is correctly anticipated by scaling laws (a) and (b) of Table 2. Finally, considering the symmetry or conceptual analogy between Tables 2 and 4, it follows that the test presented in Fig 5 validates also the theoretical results (g) and (h) listed in Table 4.

No single test is capable of validating all the heat and mass transfer scales revealed by the analysis of sections 3 and 4. Tables 2 and 4 are an invitation to additional testing, an invitation answered later in this paper in the context of boundary layer flow on the two vertical walls of a slot filled with fluid.

Note also that the scales of Table 1 and its mass transfer analogue (Table 3) need no additional testing: the scales of vertical boundary layer natural convection are amply documented in the fluid mechanics literature (see, for example, Patterson and Imberger[1]).

The boundary layer regime in a vertical slot

The reward for having determined first the scales of the boundary layer flow of Fig 1, is that now the same scales can be used to estimate the rates of heat and mass transfer across a fluid space of finite width L (Fig 6). Motivated by engineering application related to the migration of a chemical species across a double-wall space filled with fluid, we focus on convection in tall rectangular enclosures, $L/H \leqslant 1$. The problem that remains is to determine under what conditions thermal and concentration boundary layers are distinct in the vertical slot, that is, under what conditions the scales of Tables 1–4 are valid.

In their discussion of the scales of pure heat transfer in a rectangular enclosure, Patterson and Imberger[1] showed that the heat transfer scales of Table 1 apply to an enclosure heated and cooled from the side if the thermal boundary layer thickness δ_T is small compared with the horizontal dimension L:

$$\delta_T < L \tag{49}$$

in other words if:

$$\frac{L}{H} Ra^{1/4} > 1 \qquad (Pr > 1) \tag{50}$$

$$\frac{L}{H} Ra^{1/4} Pr^{1/4} > 1 \qquad (Pr < 1) \tag{51}$$

These criteria for the existence of distinct vertical boun-

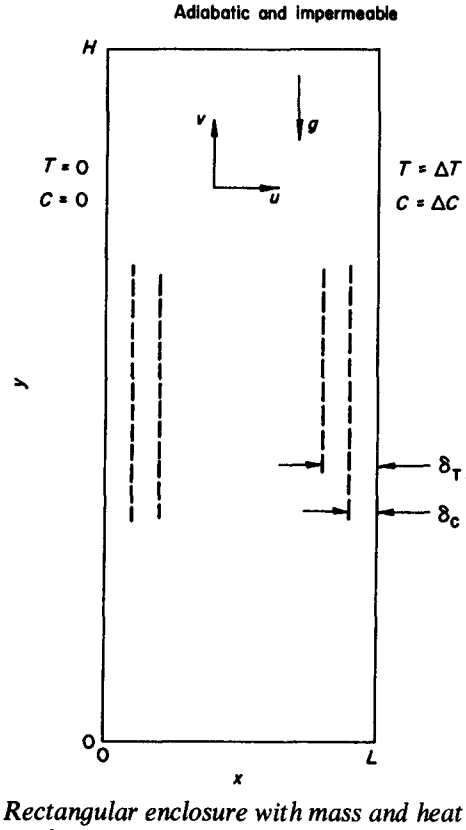

Fig 6 Rectangular enclosure with mass and heat transfer from the side

dary layers are confirmed by numerical and laboratory experiments (eg, Patterson and Imberger[1], Yewell *et al*[9]).

Based on the same reasoning, the criterion for distinct concentration boundary layers in the vertical slot of Fig 6 is:

$$\delta_C < L \tag{52}$$

which means that the mass transfer scales of Table 3 are valid for an enclosure if:

$$\frac{L}{H} Ra_m^{1/4} > 1 \qquad (Sc > 1) \tag{53}$$

$$\frac{L}{H} Ra_m^{1/4} Sc^{1/4} > 1 \quad (Sc < 1) \tag{54}$$

Criteria (49) and (52) can also be applied to the 'secondary' scales assembled in Tables 2 and 3 (these scales may be called secondary because in each case they belong to the transfer process that is insignificant with respect to driving the flow). Thus the mass transfer rate in heat-transfer-driven convection is described by the Sherwood numbers listed in Table 2 if the following conditions hold:

$$\text{(a)}\ \frac{L}{H} Le^{1/3} Ra^{1/4} > 1$$

$$\text{(b)}\ \frac{L}{H} Le^{1/2} Ra^{1/4} > 1$$

$$\text{(c)}\ \frac{L}{H} Le\, Ra^{1/4} Pr^{1/2} > 1 \tag{55}$$

$$\text{(d)}\ \frac{L}{H} Le^{1/3} Ra^{1/4} Pr^{1/12} > 1$$

$$\text{(e)}\ \frac{L}{H} Le^{1/2} Ra^{1/4} Pr^{1/4} > 1$$

$$\text{(f)}\ \frac{L}{H} Le\, Ra^{1/4} Pr^{1/4} > 1$$

Conversely, for mass-transfer-driven flows in vertical enclosures the heat transfer scales of Table 4 are valid if:

$$\text{(g)}\ \frac{L}{H} Le^{-1/3} Ra_m^{1/4} > 1$$

$$\text{(h)}\ \frac{L}{H} Le^{-1/2} Ra_m^{1/4} > 1$$

$$\text{(i)}\ \frac{L}{H} Le^{-1} Ra_m^{1/4} Sc^{1/2} > 1 \tag{56}$$

$$\text{(j)}\ \frac{L}{H} Le^{-1/3} Ra_m^{1/4} Sc^{1/12} > 1$$

$$\text{(k)}\ \frac{L}{H} Le^{-1/2} Ra_m^{1/4} Sc^{1/4} > 1$$

$$\text{(j)}\ \frac{L}{H} Le^{-1} Ra_m^{1/4} Sc^{1/4} > 1$$

If the distinct boundary layer criteria (50), (51), (53)–(56) fail, that is if the calculated δ_T, δ_C, scales are larger than L, then the actual transfer of heat or chemical species across the layer of thickness L is by diffusion. In such cases the Nusselt and Sherwood numbers for the vertical enclosure scale as:

$$Nu = \frac{Q}{k\,\Delta T} \sim \frac{kH\,\Delta T/L}{k\,\Delta T} \sim \frac{H}{L} \tag{57}$$

$$Sh = \frac{J}{D\,\Delta C} \sim \frac{DH\,\Delta C/L}{D\,\Delta C} \sim \frac{H}{L} \tag{58}$$

Tables 1–4 in association with the distinct boundary layer criteria reported here give a birds-eye-view of the combined heat and mass transfer phenomenon in a vertical slot filled with fluid, in the two extremes in which the buoyancy effect is dominated either by heat transfer or by mass transfer from the side. Relative to the multitude of transfer scales discovered in a single boundary layer (Fig 1), the heat and mass transfer scales of a vertical slot are even more numerous, due to the existence of diffusion-dominated regimes (Eqs (57) and (58)) and due to the possibility of flows with only one distinct boundary layer. This last possibility is not covered by any of the heat and mass transfer scales developed so far, and, for this reason, it forms the subject of the series of numerical experiments described next.

Numerical solutions for enclosures with only one distinct boundary layer

The series of numerical experiments reported here aims to illustrate further the effect of Lewis number on the mass transfer rate in a heat-transfer-driven flow (or on the heat transfer rate in a mass-transfer-driven flow). It is important to recognize from the start that there is more than one way in which to conduct a numerical test for the effect of Lewis number. One could start with the complete Navier-Stokes equations and vary appropriately the five dimensionless groups of the problem (Ra, N, Pr, Le, L/H) to illustrate the effect of the parameter of interest. However, this approach would be inefficient in this case because the scaling laws to be tested belong to limiting (extreme) situations in which the phenomenon is governed by equations much simpler than the Navier-Stokes equations, and the numerical results of a five-parameter problem are unable to illustrate clearly the effect of a single parameter, since each of the five parameters (whose values have to be finite) contributes its own share to the final numerical result.

A more efficient alternative is to isolate from the very start the phenomenon of interest, in this case, the mass transfer through a vertical slot in which the flow is driven by heat transfer alone. This decision amounts to setting $N=0$ in the complete momentum equation. Furthermore, since mass transfer is the phenomenon of interest and since this phenomenon does not contribute in any way to driving the flow, it makes sense to fix the temperature field and the flow field driven by it. By far the simplest choice, one that is found regularly in slender double-pane window spaces, is the diffusion temperature field

$$T = \frac{\Delta T}{L} x \tag{59}$$

and the corresponding flow field obtained by solving the flow problem:

$$0 = -\nu \nabla^2 \omega + g\beta \frac{\Delta T}{L} \tag{60}$$

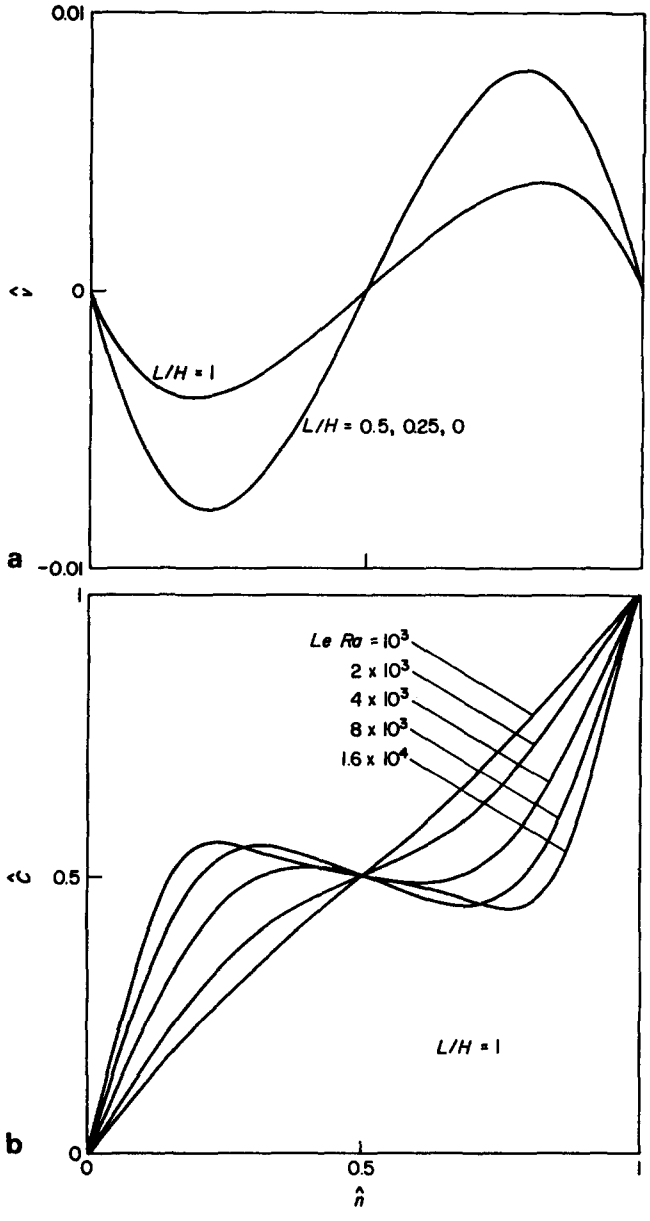

Fig 7 (a) Velocity and (b) concentration profiles in the horizontal plane situated at mid-height

$$\omega = \nabla^2 \psi \tag{61}$$

$$u = \partial\psi/\partial y \qquad v = -\partial\psi/\partial x \tag{62}$$

$$\psi = 0 \quad \text{and} \quad \frac{\partial \psi}{\partial x} = 0 \quad \text{at} \quad x = 0, L \tag{63}$$

$$\psi = 0 \quad \text{and} \quad \frac{\partial \psi}{\partial y} = 0 \quad \text{at} \quad y = 0, H \tag{64}$$

The momentum equation (60) contains the additional assumption that the Prandtl number is much larger than unity, as the inertia terms have been assumed negligible (this assumption holds even for moderate Prandtl numbers if the slot becomes tall enough, $L/H \to 0$).

In terms of the distinct boundary layer criteria presented above the flow chosen for numerical study is one without distinct thermal boundary layers:

$$\frac{L}{H} Ra^{1/4} < 1 \tag{65}$$

where $(L/H)\,Ra^{1/4}$ is finite and fixed. Since the Prandtl number is greater than one, the velocity boundary layers are not distinct also (in other words, there is no stratified core in the enclosure[10]). The vertical velocity profile is S-shaped (Fig 7) and depends only weakly on the geometric aspect ratio L/H, provided the ratio L/H is small (in fact, the velocity profiles for $L/H = 0.5$ and 0.25 are practically the same as the profile for $L/H = 0$ which is available in analytical form[11,12]).

The mass transfer phenomenon and its own transition from the diffusion regime to the concentration boundary layer regime were determined numerically using the temperature and flow fields represented by Eqs (59)–(64). The concentration field $C(x, y)$ was calculated by solving:

$$\frac{\partial \psi}{\partial y}\frac{\partial C}{\partial x} - \frac{\partial \psi}{\partial x}\frac{\partial C}{\partial y} = D\nabla^2 C \tag{66}$$

$$C = 0 \quad \text{at} \quad x = 0$$

$$C = \Delta C \quad \text{at} \quad x = L \tag{67}$$

$$\frac{\partial C}{\partial y} = 0 \quad \text{at} \quad y = 0, H$$

in which the flow field $\psi(x, y)$ is known. For numerical computation, the problems stated above were made dimensionless by introducing:

$$(\hat{x}, \hat{y}) = (x, y)/L$$

$$\hat{\omega} = \frac{\omega}{g\beta\,\Delta T L/\nu}$$

$$\hat{\psi} = \frac{\psi}{g\beta\,\Delta T L^3/\nu} \tag{68}$$

$$\hat{C} = C/\Delta C$$

In this notation, equations (60), (61) and (66) become:

$$\frac{\partial^2 \hat{\omega}}{\partial \hat{x}^2} + \left(\frac{L}{H}\right)^2 \frac{\partial^2 \hat{\omega}}{\partial \hat{y}^2} = 1 \tag{69}$$

$$\frac{\partial^2 \hat{\psi}}{\partial \hat{x}^2} + \left(\frac{L}{H}\right)^2 \frac{\partial^2 \hat{\psi}}{\partial \hat{y}^2} = \hat{\omega} \tag{70}$$

$$\frac{\partial^2 \hat{C}}{\partial \hat{x}^2} + \left(\frac{L}{H}\right)^2 \frac{\partial^2 \hat{C}}{\partial \hat{y}^2} = Le\,Ra \left(\frac{L}{H}\right)^4 \left(\frac{\partial \hat{\psi}}{\partial \hat{y}}\frac{\partial \hat{C}}{\partial \hat{x}} - \frac{\partial \hat{\psi}}{\partial \hat{x}}\frac{\partial \hat{C}}{\partial \hat{y}}\right) \tag{71}$$

showing that the flow field depends on L/H alone, and that the concentration field depends on L/H and $Le\,Ra(L/H)^4$. The dimensionless form of the boundary conditions (63), (64) and (67) is not listed, for the sake of brevity.

Eqs (69)–(71) were approximated via the standard centred finite difference method and solved iteratively on the computer. The method was identical to one used earlier in the study of natural convection in a vertical porous layer saturated with fluid[13]: note that Eqs (67)–(71) are of the same type as in Darcy flow natural convection. Grid fineness tests documented in the earlier study and repeated here showed that the uniform grid size $\Delta x = \Delta y = L/20$ is fine enough to yield overall Sherwood number results within one percent of the asymptotic value. Thus, the results reported in Table 6 were obtained using a mesh with 21×21 lines for $L/H = 1$, 21×41 for $L/H = 0.5$, and 21×81 for $L/H = 0.25$. The boundary

Table 6 Numerical results for mass transfer via heat-transfer-driven natural convection in a vertical slot ($N=0$, $Pr \gg 1$, $(L/H)Ra^{1/4} \ll 1$).

L/H	$Le\,Ra$	$\frac{L}{H}Sh$	$\hat{\psi}_{max}$
1	10^3	1.134	1.26×10^{-3}
	1.5×10^3	1.272	
	2×10^3	1.426	
	2.5×10^3	1.580	
	3×10^3	1.723	
	3.5×10^3	1.855	
	4×10^3	1.973	
	4.5×10^3	2.080	
	5×10^3	2.178	
	5.5×10^3	2.267	
	6×10^3	2.350	
	6.5×10^3	2.427	
	7×10^3	2.500	
	8×10^3	2.635	
	10^4	2.875	
	1.6×10^4	3.495	
	2×10^4	3.800	
0.5	5×10^3	1.054	2.60×10^{-3}
	10^4	1.191	
	2×10^4	1.543	
	4×10^4	2.122	
	8×10^4	2.786	
0.25	2×10^4	1.0035	2.61×10^{-3}
	4×10^4	1.0136	
	8×10^4	1.048	
	1.6×10^5	1.142	
	3.2×10^5	1.338	
	6.4×10^5	1.714	

conditions for vorticity and zero mass flux along the top and bottom walls were based on three-node approximations. Likewise, the local mass flux along the vertical walls was calculated using a three-node approximation for the concentration gradient normal to the wall. Table 6 shows the resulting value of the overall Sherwood number defined by Eq (14): it is worth noting that the group $Sh\,L/H$ is the diffusion-referenced Sherwood number whose value is one in the regime delineated by criterion (58).

Fig 8 shows the overall Sherwood number calculations as $Sh\,L/H$ versus L/H and the combined group $Le\,Ra(L/H)^4$. Firstly, this figure shows that the aspect ratio L/H has only a minor effect if the vertical slot is slender, as suggested already by the non-dimensionalized equations (67)–(71). The same figure also validates the method of scale analysis on which results (a) and (b) of Table 2 and (g) and (h) of Table 3 are based. To see this, it is necessary to keep in mind that the mass transfer regime documented by the experiments of Fig 8 does not conform to the boundary layer regimes represented by cases (a), (b), (g) and (h), because in the present case the flow is one without distinct velocity boundary layers (wall jets). As shown in Fig 7, the vertical velocity profile is a counterflow in which the transversal scale of each stream is of order L and, from Eq (68), the peak vertical velocity scale is of order:

$$v \sim \frac{g\beta\,\Delta T L^2}{\nu} \tag{72}$$

The scale analysis presented earlier for cases (a) and (b) can be repeated using Eq (72) as peak vertical velocity scale instead of the boundary layer velocity scale listed in Table 1 for $Pr>1$. And, as shown by the concentration boundary layer profiles of Fig 7, we have two cases to consider:

Case (a'): $\delta_C < L$

In this case the vertical velocity in the δ_C-thick layer is of order $(\delta_C/L)v$, with the v scale given by Eq (72). Repeating the analysis between Eqs (15) and (18) we obtain:

$$\frac{L}{H}Sh \sim \left[Le\,Ra\left(\frac{L}{H}\right)^4\right]^{1/3} \tag{73}$$

Case (b'): $\delta_C \sim L$

When the concentration boundary layer penetrates through the vertical stream, the vertical velocity scale in the δ_C-thick layer is the same as in Eq (72); omitting the algebra, the equivalent of the analysis contained between Eqs (21) and (25) yields:

$$\frac{L}{H}Sh \sim \left[Le\,Ra\left(\frac{L}{H}\right)^4\right]^{1/2} \tag{74}$$

Scaling results (73) and (74) indicate that on a graph such as Fig 8 the diffusion referenced Sherwood number should pass through three different regimes:

I. At very low values of the abscissa parameter, when the concentration layer is not distinct, $Sh\,L/H$ should be asymptotically equal to one.
II. At intermediate values of $Le\,Ra(L/H)^4$, ie when $\delta_C \sim L$, the diffusion-referenced Sherwood number should increase as the square root of the abscissa parameter, Eq (74).
III. At high values of $Le\,Ra(L/H)^4$, when δ_C is much smaller than L, the slope of the $Sh\,L/H$ curve on Fig 8 must be 1/3 (Eq (73)).

These three features are confirmed without ambiguity by the overall Sherwood number data of Table 6 and Fig 8. The agreement between the theoretical features I–III, and numerical experiments confirms that the method of scale analysis employed above is correct and, more specifically, that in the transition from regime (a) to (b) the Sherwood number dependence on Lewis number shifts from $Le^{1/3}$ to $Le^{1/2}$. This last statement reinforces the test constructed in Fig 5, especially since prior to this study the existence of a $Le^{1/3}$-dependence for Sherwood number was not recognized in the natural convection mass transfer literature.

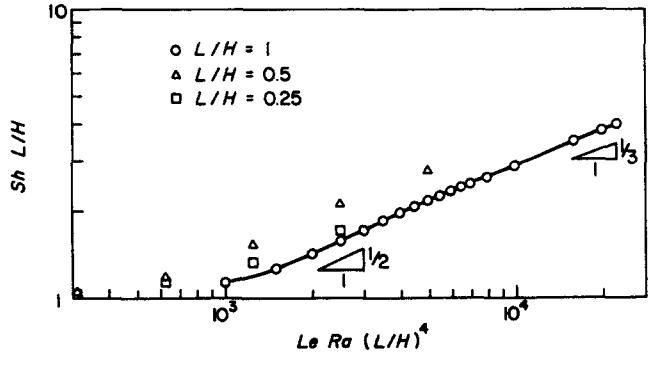

Fig 8 Numerical results for overall mass transfer through a vertical cavity (N=0, Pr>1, (L/H) $Ra^{1/4}<1$)

Acknowledgement

This study was supported by the National Science Foundation through Grant No. MEA-82-07779. The present report was prepared during the author's term as F. Mosey Visiting Scholar to the Faculty of Engineering, and with the support of the Centre for Environmental Fluid Dynamics, University of Western Australia.

References

1 **Patterson J. C. and Imberger J.** Unsteady natural convection in a rectangular cavity, *J. Fluid Mech., 1980,* **100**, *65*

2 **Blythe P. A., Daniels P. G. and Simpkins P. G.** Thermally driven cavity flow in porous media: I. The vertical boundary layer structure near the corners, *Proc. Roy. Soc., 1982,* **A380**, *119*

3 **Somers E. V.** Theoretical considerations of combined thermal and mass transfer from a vertical flat plate, *J. Appl. Mech., 1956,* **23**, *295*

4 **Mathers W. G., Madden A. J. and Piet E. L.** Simultaneous heat and mass transfer in free convection, *Ind. Eng. Chem., 1957,* **49**, *961*

5 **Wilcox W. R.** Simultaneous heat and mass transfers in free convection, *Chem. Eng. Sci., 1961,* **13**, *120*

6 **deLeeuw Den Bouter J. A., DeMunnik B. and Heertjes P. M.** Simultaneous heat and mass transfer in laminar flow convection from a vertical plate, *Chem. Eng. Sci., 1968,* **23**, *1185*

7 **Gebhart B. and Pera, L.** The nature of vertical natural convection flows resulting from the combined buoyancy effects of thermal and mass diffusion, *Int. J. Heat Mass Transfer, 1971,* **14**, *2025*

8 **Bejan A. and Cunnington G. R.** Theoretical considerations of transition to turbulence in natural convection near a vertical wall, *Int. J. Heat and Fluid Flow, 1983,* **4**, *131*

9 **Yewell R., Poulikakos D. and Bejan A.** Transient natural convection experiments in shallow enclosures, *J. Heat Transfer, 1982,* **104**, *533*

10 **Gill A. E.** The boundary layer regime for convection in a rectangular cavity, *J. Fluid Mech., 1966,* **26**, *515*

11 **Batchelor G. K.** Heat transfer by free convection across a closed cavity between vertical boundaries at different temperature, *Quart. Appl. Math., 1954,* **12**, *209*

12 **Rohsenow, W. M. and Choi, H. Y.** *Heat, Mass and Momentum Transfer, Prentice-Hall, Englewood Cliffs, New Jersey, 1961, Chapter 7*

13 **Bejan A.** Natural convection heat transfer in a porous layer with internal flow obstructions, *Int. J. Heat Mass Transfer, 1983,* **26**, *815*

BOOK REVIEW

Engineering Flow and Heat Exchange

O. Levenspiel

This book is designed to be used in a course following on from one that introduces the principles of heat, mass and momentum transfer and not much more.

The first half of the book is entitled 'Flows of fluids and mixtures'. In eight chapters, this covers basic fluid mechanics for flows that are Newtonian and non-Newtonian, compressible and incompressible, and the specialized topics of terminal velocities, low pressure systems as well as flows through packed and fluidized beds. The second half, 'Heat Exchange', takes the student through basic heat transfer plus through-the-wall and direct heat exchangers as well as energy storage devices. Radiation heat transfer is given only a brief introduction.

In the author's preface, he states that the book will be of interest to practising engineers or technologists who want a broad picture of the subject or who need help in getting started on the solution to a problem. In this respect I think the book serves its purpose. One can see how someone who is a technologist or engineer in a field other than chemical or mechanical engineering could find the book quite useful. Such users may well want to go further with a problem than is possible by using this book. Here, the references are adequate support for the material discussed. To be of much use as a book for non-experts, however, a bibliography of newer, specialized books on heat exchangers, fluidized beds and the like would be most useful.

The second suggested application of the book, as alluded to in the first paragraph above, is as a follow-on text. Here it could not be used after typical texts on transport phenomena as there would be far too much overlap in most areas. It would best fit in as a service course for other than chemical or mechanical engineers or technologists. For instance, I can see it following *Engineering Thermodynamics* by Reynolds and Perkins or *Introduction to Thermal Sciences* by Schmidt *et al*, although the second is probably already too comprehensive.

Subject to the above restrictions, the book is well written and the examples as well as the problems after each chapter are interesting and instructive.

C. J. Cremers
University of Kentucky,
Lexington, KY,
USA

Published, price $34.50, by Plenum Press, 233 Spring Street, New York, NY 10013, USA